Optics Letters

Blueshift and phase tunability in planar THz metamaterials: the role of losses and toroidal dipole contribution

Maria V. Cojocari, Kristina I. Schegoleva, and Alexey A. Basharin*

National University of Science and Technology (MISiS), Laboratory of Superconducting Metamaterials, 119991 Moscow, Russia
**Corresponding author: alexey.basharin@gmail.com*

Received 27 February 2017; revised 17 March 2017; accepted 23 March 2017; posted 28 March 2017 (Doc. ID 287550); published 20 April 2017

We propose a model of tunable THz metamaterials. The main advantage is the blueshift of resonance and phase tunability due to inductive coupling in planar metallic metamolecules with incorporated silicon wires. We discuss the role of losses and toroidal dipole contribution to metamaterial response.

OCIS codes: (160.3918) Metamaterials; (250.4110) Modulators.

https://doi.org/10.1364/OL.42.001700

Metamaterials are artificial structures with properties unattainable in natural media. Their exotic response is a promising platform for filling the THz frequency gap [1–3]. A separate class of metamaterials is the one with the toroidal response [4–16]. The toroidal observation is mediated by the excitation of currents flowing in inclusions of toroidal metamolecules and resembles the poloidal currents along the meridians of a gedanken torus [4,5]. Such closed fields configuration determines the high Q-factor of toroidal metamaterials [14–18]. Meanwhile, the destructive interference between the toroidal and electric dipole moments leads to a lack in the far-fields, but the fields in the metamolecule origin are described by δ-function [6,7]. Such fields configuration, referred to as anapole, allows for observation of the new effect of electromagnetically induced transparency (EIT) [6,7], which provides an extremely high Q-factor in metamaterials [8], enables cloaking for nanoparticles [9,10], and is a platform for confirmation of the dynamic Aharonov–Bohm effect [6,7].

Recently, the anapole excitation was demonstrated in planar metamaterials, which enabled an extremely high Q-factor in microwave [8]. This gives promising opportunities for tunable metamaterials due to the strong electromagnetic fields localization within metamolecules. In this Letter, we consider the design of a metamaterial, discussed in [8], in the tunable regime. For this purpose, we incorporate the photoconductive silicon into the metamolecule [Fig. 1(a)] and study the metamaterial response in the THz regime. The silicon is simulated with the pump-power-dependent conductivity σ_{Si}, which means transition from dielectric to metallic state.

Metamolecules comprise two split parts [Fig. 1(a)]. The incident plane electromagnetic wave with electric field $\boldsymbol{E}$ aligned with the central wire excites conductive currents in each loop of the metamolecule. The currents form a closed vortex of magnetic field $\boldsymbol{H}$. As a result, such configuration of electromagnetic fields supports the toroidal dipole excitation, oscillating upward and downward within the metamolecule. However, the electric dipole also arises in the metamolecule and maintains the interference between electric and toroidal dipole moments. For the first time, we consider here how the planar toroidal metamolecule can be exploited as a building block for THz modulators. We demonstrate the blueshift and the phase tunability regime and also discuss the role of losses.

The metamaterials with incorporated silicon or gallium arsenide inclusions were discussed in detail as elements of modulators. The phase tunability, blueshift, redshift, as well as amplitude switching, have been shown in THz frequency range [18–27]. Although the semiconductor inclusions play the role of capacitor elements or as the tunable metamaterial substrate, our advantage is related to inductive tunability achieved by changing of the silicon conductivity. This configuration introduces additional inductance in the metamolecule, and, because of increasing of silicon conductivity, we expect blueshift of resonance frequency by currents flowing along silicon strips [Fig. 1(c)] instead of those along external metallic parts of the metamolecule [Fig. 1(b)]. Such incorporation of silicon decreases the electric dimensions of metamolecules.

The electromagnetic properties of metamaterial are computed by commercial Maxwell's equation solver HFSS. We suppose that all metamolecules are periodically arranged in

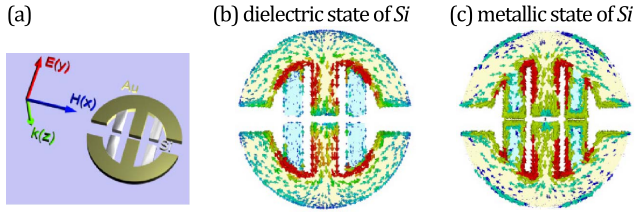

Fig. 1. (a) Illustration of the proposed metamolecule, supporting the toroidal and electric dipolar excitation with incorporated silicon strips. The diameter of the metamolecule is 30 μm, with central gap equal to 2 μm and the lateral gaps 5 μm. The silicon strips have the 1.4 μm gaps. (b) Conductive currents on the frequency 4.56 THz and for period $D = 37$ μm. (c) Conductive currents on the frequency 5.39 THz.

x and y directions with $D = 37$ μm center-to-center separation. We study gold metamolecules with conductivity $\sigma_{gold} = 7 \times 10^6$ S/m. During our simulation, we consider a single unit cell [Fig. 1(a)], with electromagnetic incident wave in z-direction and periodic boundary conditions. For the tunable silicon area, we set permittivity of silicon $\varepsilon_{Si} = 11.9$ and conductivity σ_{Si} varying from 10^{-1} S/m to 10^6 S/m. Figure 2(a) shows the simulated transmission spectra for different conductivities of silicon. For small conductivities, silicon is purely dielectric. Without pump beam, the transmission minimum is characterized by resonance dip in vicinity of 4.84 THz. With increasing conductivity, the resonance is initially unchanged ($\sigma_{Si} < 10^3$ S/m) [Fig. 3(b)]. Since $\sigma_{Si} = 10^3$ S/m, we observe blueshift accompanied by increasing transmission intensity and attainable 5.25 THz on the 10^5 S/m. Finally, for the metallic state of silicon $\sigma_{Si} = 10^6$ S/m, the transmission resonance achieves the maximum shift of 5.39 THz [Figs. 2(a) and 3(b)], while the phase perturbation during σ_{Si} variations is negligibly small [Fig. 2(b)]. We note that such blueshift appears because of the contribution of silicon inclusions in overall distribution of currents. At low conductivities ($\sigma_{Si} < 10^3$ S/m), the currents flow along metallic parts of metamolecules [Fig. 1(b)], but with the transition to the metallic state ($\sigma_{Si} > 10^3$ S/m), currents flowing along the silicon inclusions are dominating [Fig. 1(c)]. This corresponds to the decrease in electric size of the metamolecule and to the blueshift of resonance frequency from 4.84 THz to 5.39 THz (Fig. 2).

To evaluate the role of multipoles in resonance formation, we consider the power of the five strongest multipoles calculated from conductive and displacement currents extracted from the simulations [Fig. 3(a)]. For calculation of multipoles powers, we use the approach established in Ref. [16]. We plot normalized power radiated by electric **P**, magnetic **M**, toroidal **T**, electric quadropole **Qe**, and magnetic quadropole **Qm** moments, corresponding to transmission dips depicted in Fig. 2(a) and dependent on silicon conductivities σ_{Si}. For low pump illumination, the silicon is purely dielectric, and resonance is mainly defined by electric and toroidal multipoles. However, with the increase of σ_{Si}, the decomposition between moments occurs, and the electric moment will dominate more strongly. Intensities of other multipoles are less than 100 times as compared with electric and toroidal moments. Moreover, a significant difference between the electric and toroidal dipoles explains low Q-factor at frequencies ~5.39 THz and $\sigma_{Si} > 10^4$ S/m compared with the higher Q-factor dip on the frequencies ~4.84 THz and $\sigma_{Si} < 10^4$ S/m, for which the electric and toroidal dipoles have intensities very close to each other. Thus, we observe the blueshifted Fano-type resonance, which is varied by transition of silicon conductivity from dielectric to metallic state. We can expect that higher tunability may be achieved by optimization of our structure. For example, the elliptical shape of the metamolecule elongated along the x-axis instead of a circular one allows for the increase in the metamolecule size. Thus, the resonance moves (for $\sigma_{Si} = 0$ S/m) to lower frequencies, which will increase blueshift capability. In addition to the inductive coupling, we may supplement the capacitive one: expanding the gaps of silicon wires, which gives us an extra degree of freedom for manipulations.

Interestingly, the proposed metamaterial can exhibit the phase tunability. For this purpose, we assume the distance between metamolecules centers to be $D = 30$ μm. At low conductivities of silicon σ_{Si}, pronounced peak is significantly reduced to 0.5 [Fig. 4(a)]. With growth of conductivity σ_{Si} one cannot be distinguished from the overall transmission curve close to the 6.5 THz. Thus, it is impossible that the amplitude tunability is caused by resonance. However, we can make an assumption here. Dissipative losses in the metamolecules influence the transmission amplitude, whereas large phase tunability is observed in order to transition from the dielectric state of silicon to the metallic state (see the summary later in this

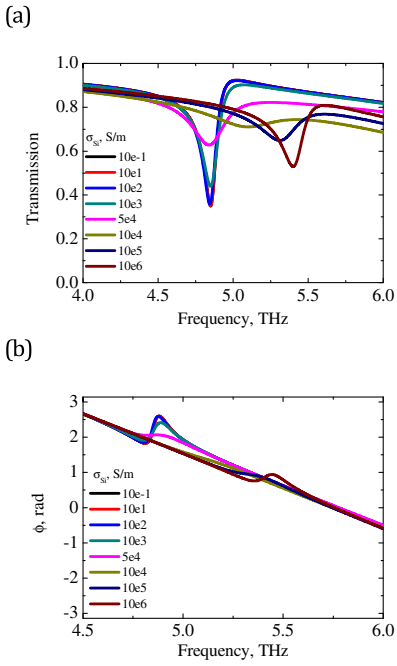

Fig. 2. Simulated transmission spectra for different conductivities of silicon for the period of metamolecules $D = 37$ μm (a) intensities and (b) phases.

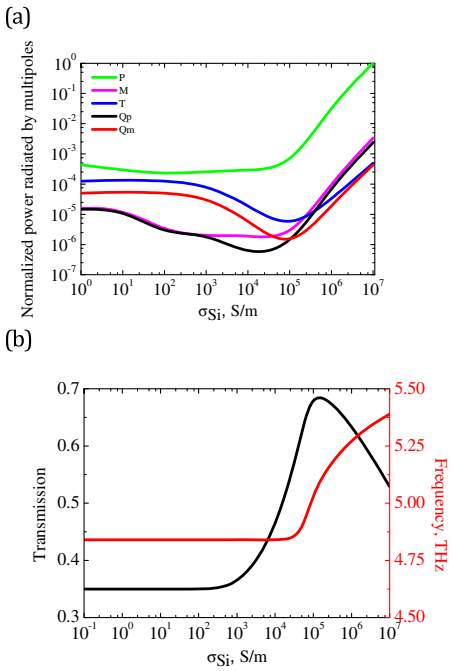

Fig. 3. (a) Contributions of the five strongest multipolar excitations to the electromagnetic response from metamaterial sample in log scale for the case of period $D = 37$ μm and (b) the transmission and resonance frequency dependent on silicon conductivity σ_{Si}.

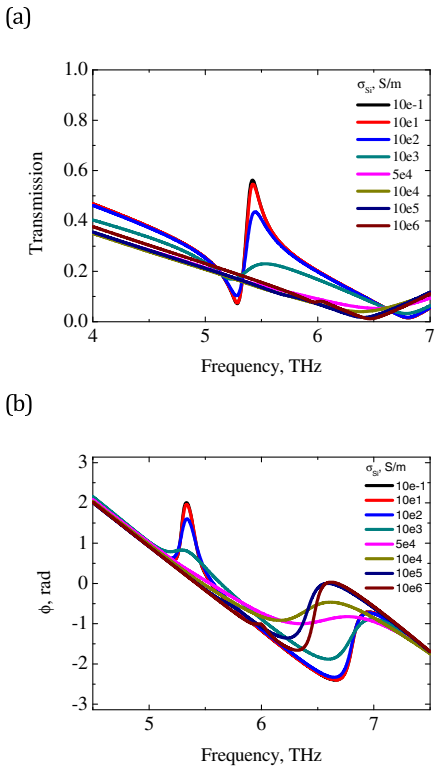

Fig. 4. Simulated transmission spectra for different conductivities of silicon for the period of metamolecules $D = 30$ μm (a) intensities and (b) phases.

Letter). We achieve tunability ~2 rad, which is the benefit of proposed metamaterial as a platform for THz phase modulators (Fig. 5). Indeed, the variation of silicon conductivity σ_{Si} from 1 S/m to 10^6 S/m significantly changes the phase from −2 to 0 rad, associated with nondisturbing intensity in broad frequency range from 6.5 to 7.2 THz [Figs. 4(a) and 4(b)]. Moreover, in Fig. 5, we generalize the tunability characteristics. We show the contribution of conductivity σ_{Si} on the transmission phase and amplitude at 6.6 THz. For low conductivities ($<10^3$ S/m), the phase shift is almost a constant. The significant phase shift occurs for $\sigma_{Si} > 10^3$ S/m, which is linearly enhanced up to 10^6 S/m, whereas the transmission amplitude is constant and very low during the σ_{Si} variation.

However, the phase modulation effect can be exploited in the reflection regime, similar to the phase tunable mirror [28]. In this case, the reflection will be very high ($R = 1 - T$).

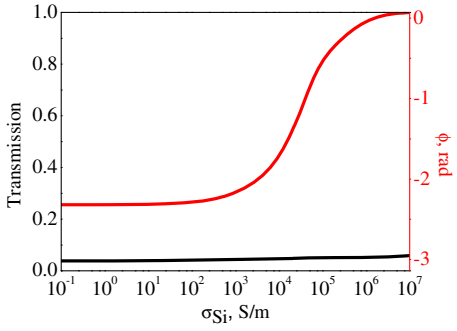

Fig. 5. Amplitude and phase tunability dependent on silicon conductivity σ_{Si} on the 6.5 THz for metamaterial with the period $D = 30$ μm.

Importantly, we also discuss the role of multipoles in forming the phase tunability. Indeed, the contributions of all multipoles are the same for varied conductivities σ_{Si}, the electric dipole moment dominates, and toroidal intensities are very high in comparison with other multipoles at the frequency of 6.6 THz [Fig. 6(a)] during the σ_{Si}, evaluation. Moreover, the phase behavior [Fig. 6(b)] of toroidal and electric dipoles reminds one of the graph in Fig. 5. Therefore, the main origin of the phase tunability is the phase manner of multipoles instead of their amplitude. Thus, the achieved phase tunability is very high, ~2 rad. We expect that our metamaterial would operate with low pump intensity without high power sources because we need to act only on small silicon wires.

As the summary, we discuss the role of losses in proposed metamaterials. The actual losses of metals in the THz frequency range can be crucial for discussed effects. Although metals in the microwave range can be considered as perfect electric conductor (PEC), the real conductivities in the THz region limit the Q-factor and destroy the high-Q resonances. We represent in Fig. 7 the amplitude and phase tunability for the proposed metamaterial with $D = 30$ μm. We plot the graph for varied conductivity of metamolecules material σ_{met}, where $\Delta A = |A_{dielectric} - A_{metallic}|$ and $\Delta\phi = |\phi_{dielectric} - \phi_{metallic}|$ are intensities and phases characterizing the tunability or the difference between metallic and dielectric state of silicon. Decrease of σ_{met} reduces the resonance intensity, while the phase tunability is evident. It implies that the dissipative losses destructively affect the transmission amplitude, while phase tunability is crucial for real conductivities of metals in THz regime ($\sigma_{met} < 10^8$ S/m), and amplitude tunability is lacking in this case. This explains

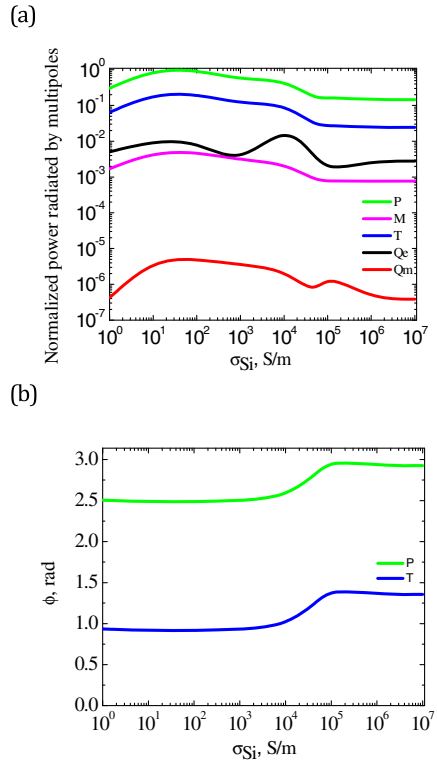

Fig. 6. (a) Contributions of the five strongest multipolar excitations to the electromagnetic response from metamaterial sample in log scale for $D = 30$ μm. (b) The phases of the electric and the toroidal dipole moments versus frequency.

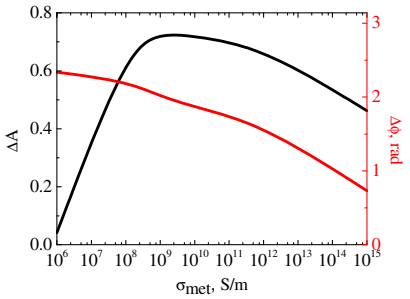

Fig. 7. Simulated tunability of intensity and phase difference of electromagnetic wave passed through a metamaterial sample dependent on metamolecules conductivity σ_{met} for the period $D = 30$ μm.

why we observe significant phase tunability ~2 rad on Fig. 4(b) without amplitude tunability [Figs. 4(a) and 5].

It is well known that the metamaterial response is limited by radiating and nonradiating losses. Q-factor of metamaterials is described as $Q = 1/Q_{rad} + 1/Q_{non}$, where Q_{rad} is radiating losses and Q_{non} is nonradiating or dissipative losses. While the radiating losses in toroidal metamaterials are low, we are limited mainly by Joule losses in ingredients, which can be compensated by exploiting superconducting or dielectric inclusions. However, this formula addresses that we have the background for playing between Q_{rad} and Q_{non}. Indeed, negligible mismatch between multipoles leads to the decreasing of Q_{rad}, but Q_{non} has some frame for manipulation of losses in order to enhance the Q-factor. This fact explains why the transmission resonance for $D = 37$ μm [Fig. 2(a)] has higher Q than for $D = 30$ μm [Fig. 4(a)]. In this way, we enhanced the radiation losses and, as a result, the interaction among electric, toroidal, and other multipoles.

Let us compare our idea with other papers about inductive coupling. The first approach is concerned with the switching of extra parts of hybrid split ring resonator (SRR) [21]. The multilayer UV lithography was applied for fabrication of the switching element by deposition of the semiconductor on the top of the SRR gap [21] and as the "elongating" element for the metamolecules to increase their inductance [29,30]. The second approach is based on the graphene exploited as a metamaterial substrate and also as a switching element in the inclusion itself, leading to both phase modulation [28,31] and blueshift tunability [32]. Moreover, the phase modulation is organized by dynamic photoexcitation of metamaterials substrate [22] or by applying external voltage for control carrier density in a metal-semiconductor zone [19]. However, our idea shows promise primarily because of the possibility of phase modulation not requiring the graphene or thick semiconductor substrates.

Recently, planar metamaterials with toroidal contribution have attracted attention because of the high Q-factor. Nevertheless, the nonradiative losses can be crucial in the THz regime. These metamaterials are promising for tunability because of coupling effects between multipoles. Here, we extend our previous design [8] as metamaterials with inductive coupling. The role of losses, multipoles contribution, and inductive tunability was demonstrated. We believe that our approach paves the way for future THz modulators showing deep blueshift and phase tunability realized because of the change of semiconductor conductivity.

Funding. Ministry of Education and Science of the Russian Federation (Minobrnauka), NUST "MISiS" (K4-2015-031); Russian Foundation for Basic Research (RFBR) (16-32-50139, 16-02-00789).

REFERENCES

1. W. J. Padilla, A. J. Taylor, C. Highstrete, M. Lee, and R. D. Averitt, Phys. Rev. Lett. **96**, 107401 (2006).
2. H.-T. Chen, W. J. Padilla, J. M. O. Zide, A. C. Gossard, A. J. Taylor, and R. D. Averitt, Nature **444**, 597 (2006).
3. W. Withayachumnankul and D. Abbott, IEEE Photon. J. **1**, 99 (2009).
4. T. Kaelberer, V. A. Fedotov, N. Papasimakis, D. P. Tsai, and N. I. Zheludev, Science **330**, 1510 (2010).
5. N. Papasimakis, V. A. Fedotov, V. Savinov, T. A. Raybould, and N. I. Zheludev, Nat. Mater. **15**, 263 (2016).
6. V. A. Fedotov, A. V. Rogacheva, V. Savinov, D. P. Tsai, and N. I. Zheludev, Sci. Rep. **3**, 2967 (2013).
7. N. A. Nemkov, A. A. Basharin, and V. A. Fedotov, "Non-radiating sources, dynamic anapole and Aharonov-Bohm effect," arXiv:1605.09033 (2016).
8. A. A. Basharin, V. Chuguevsky, N. Volsky, M. Kafesaki, and E. N. Economou, Phys. Rev. B **95**, 035104 (2017).
9. A. A. Basharin, M. Kafesaki, E. N. Economou, C. M. Soukoulis, V. A. Fedotov, V. Savinov, and N. I. Zheludev, Phys. Rev. X **5**, 011036 (2015).
10. A. E. Miroshnichenko, A. B. Evlyukhin, Y. F. Yu, R. M. Bakker, A. Chipouline, A. I. Kuznetsov, B. Luk'yanchuk, B. N. Chichkov, and Y. S. Kivshar, Nat. Commun. **6**, 8069 (2015).
11. A. C. Tasolamprou, O. Tsilipakos, M. Kafesaki, C. M. Soukoulis, and E. N. Economou, Phys. Rev. B **94**, 205433 (2016).
12. A. B. Evlyukhin, T. Fischer, C. Reinhardt, and B. N. Chichkov, Phys. Rev. B **94**, 205434 (2016).
13. H. Xiang, L. Ge, L. Liu, T. Jiang, Z. Q. Zhang, C. T. Chan, and D. Han, Phys. Rev. B **95**, 045403 (2017).
14. Y. Fan, Z. Wei, H. Li, H. Chen, and C. M. Soukoulis, Phys. Rev. B **87**, 115417 (2013).
15. M. Gupta, V. Savinov, N. Xu, L. Cong, G. Dayal, S. Wang, W. Zhang, N. I. Zheludev, and R. Singh, Adv. Mater. **28**, 8206 (2016).
16. V. Savinov, V. A. Fedotov, and N. I. Zheludev, Phys. Rev. B **89**, 205112 (2014).
17. Z. Liu, S. Du, A. Cui, Z. Li, Y. Fan, S. Chen, W. Li, J. Li, and C. Gu, Adv. Mater. (2017), doi: 10.1002/adma.201606298.
18. Y. Fan, F. Zhang, Q. Fu, Z. Wei, and H. Li, "Controlling the toroidal excitations in metamaterials for high-Q response," arXiv: 1609.05804 (2016)
19. H.-T. Chen, W. J. Padilla, M. J. Cich, A. K. Azad, R. D. Averitt, and A. J. Taylor, Nat. Photonics **3**, 148 (2009).
20. N.-H. Shen, M. Kafesaki, T. Koschny, L. Zhang, E. N. Economou, and C. M. Soukoulis, Phys. Rev. B **79**, 161102(R) (2009).
21. N.-H. Shen, M. Massaouti, M. Gokkavas, J.-M. Manceau, E. Ozbay, M. Kafesaki, T. Koschny, S. Tzortzakis, and C. M. Soukoulis, Phys. Rev. Lett. **106**, 037403 (2011).
22. J.-M. Manceau, N.-H. Shen, M. Kafesaki, C. M. Soukoulis, and S. Tzortzakis, Appl. Phys. Lett. **96**, 021111 (2010).
23. X. Shen and T. J. Cui, J. Opt. **14**, 114012 (2012).
24. O. Buchnev, J. Wallauer, M. Walther, M. Kaczmarek, N. I. Zheludev, and V. A. Fedotov, Appl. Phys. Lett. **103**, 141904 (2013).
25. D. R. Chowdhury, R. Singh, A. J. Taylor, H.-T. Chen, and A. K. Azad, Appl. Phys. Lett. **102**, 011122 (2013).
26. X. Zhao, K. Fan, J. Zhang, G. R. Keiser, G. Duan, R. D. Averitt, and X. Zhang, Microsyst. Nanoeng. **2**, 16025 (2016).
27. M. Kafesaki, N. H. Shen, S. Tzortzakis, and C. M. Soukoulis, J. Opt. **14**, 114008 (2012).
28. Z. Miao, Q. Wu, X. Li, Q. He, K. Ding, Z. An, Y. Zhang, and L. Zhou, Phys. Rev. X **5**, 041027 (2015).
29. G. Kenanakis, R. Zhao, N. Katsarakis, M. Kafesaki, C. M. Soukoulis, and E. N. Economou, Opt. Express **22**, 12149 (2014).
30. Y. Fan, T. Qiao, F. Zhang, Q. Fu, J. Dong, B. Kong, and H. Li, Sci. Rep. **7**, 40441 (2017).
31. S. Arezoomandan and B. Sensale-Rodriguez, in *39th International Conference on Infrared, Millimeter, and Terahertz Waves (IRMMW-THz)* (2014).
32. S. H. Mousavi, I. Kholmanov, K. B. Alici, D. Purtseladze, N. Arju, K. Tatar, D. Y. Fozdar, J. W. Suk, Y. Hao, A. B. Khanikaev, R. S. Ruoff, and G. Shvets, Nano Lett. **13**, 1111 (2013).